# LABORATOIRE NATIONAL SATURNE



91191 Gif-sur-Yvette Cédex France

## A MODIFIED SPACE CHARGE ROUTINE FOR HIGH INTENSITY BUNCHED BEAMS

P. Lapostolle*, A.M. Lombardi**, E. Tanke**, S. Valero***,
R.W. Garnett****, T.P. Wangler****

* *Consultant, PS Division CERN, CH-1211 Geneva 23, Switzerland*
** *PS Division CERN, CH-1211 Geneva 23, Switzerland*
*** *DSM-CEA & IN2P3-CNRS, LNS, CE-Saclay, F-91191 Gif-sur-Yvette Cedex, France*
**** *Los Alamos National Laboratory, Los Alamos, NM 87545, USA*

*CEA/DSM/GECA/GT/96-01*

Centre National de la Recherche Scientifique
Commissariat à l'Energie Atomique

# A MODIFIED SPACE CHARGE ROUTINE FOR HIGH INTENSITY BUNCHED BEAMS

P. Lapostolle*, A.M. Lombardi**, E. Tanke**, S. Valero***,
R.W. Garnett****, T.P. Wangler****

* *Consultant, PS Division CERN, CH-1211 Geneva 23, Switzerland*
** *PS Division CERN, CH-1211 Geneva 23, Switzerland*
*** *DSM-CEA & IN2P3-CNRS, LNS, CE-Saclay, F-91191 Gif-sur-Yvette Cedex, France*
**** *Los Alamos National Laboratory, Los Alamos, NM 87545, USA*

## INTRODUCTION

Present linac beam dynamics codes normally include a space charge routine, describing the evolution of intense beams. They find their application in accelerators used as injectors for ultra high energy machines applied in particle physics research. A new generation of linacs is now under consideration for various industrial applications like fission products waste incineration, generation of electrical power, pulsed neutron research facilities and other developments on advanced materials. What is needed in such machines is maintaining the loss level at less than 1 W/m. Therefore theories are now being developed to understand and quantify the mechanisms of the formation of the beam halo. Simulations codes are being improved for more detailed study of the exact beam evolution, with the aim to reduce some of the difficulties of the present space charge routines.

The present work, with its flexibility, is a step in this direction with the aim to reduce some of the difficulties of the present routines. It is now introduced in the new beam dynamics code DYNAC [1]. The new beam dynamics method used in this code, employs a set of quasi-Liouvillian equations, allowing beam dynamics computations in long and complex structures for electrons, as well as protons and ions. With this new beam dynamics method, the coordinates of particles are known at any position in the accelerating elements, allowing multistep space charge calculations.

## I. SPACE CHARGE COMPUTATIONS IN HIGH INTENSITY BUNCHED BEAMS

The space charge forces in a numerical simulation of a charged particle beam are calculated by computing the Coulomb interactions between point like macroparticles.

Several methods have been developed : space charge routines can be classified in three categories.

The first type is a Particle to Particle Interaction (PPI) procedure. Here the space charge field is often made linear inside spherical clouds of an optimised size around each macroparticle and according to Coulomb interaction outside these clouds. As these methods are strongly subject to statistical noise, they require a great number of macroparticles. Their main disadvantage is that they are very time consuming on the computer. Increasing the number of macroparticles M, the computing time increases as $M^2$.

The second type makes use of Particle In Cell (PIC) codes : the space charge potential is computed on the nodes of a mesh superimposed on the bunch, with an adequate smoothing interpolation from node to node. Further on a description of one of these procedures can be found. In order to avoid the long computing time and large amount of memory required for 3-d calculations, most routines use rotational symmetry of the particle distribution around the axis for the computation. As a consequence this method has as a disadvantage that it is restricted to those locations where the transverse beam cross section is roughly round. These routines can also be subject to statistical noise as will be shown.

In the last type one assumes that in transverse and longitudinal directions, the bunches keep an elliptical distribution. Such an assumption, reasonable in the transverse direction, is not justified in the longitudinal direction where the motion is governed by a non-linear equation different from the one acting in the transverse direction. The longitudinal beam density distribution can take a complex non-symmetrical form ( fig. 1 ), whereas in the transverse direction it generally keeps a simpler symmetrical shape. The new method is a modified version of this last type : considering bunches to be consisting of several ellipsoids, it can treat a non-symmetrical longitudinal distribution.

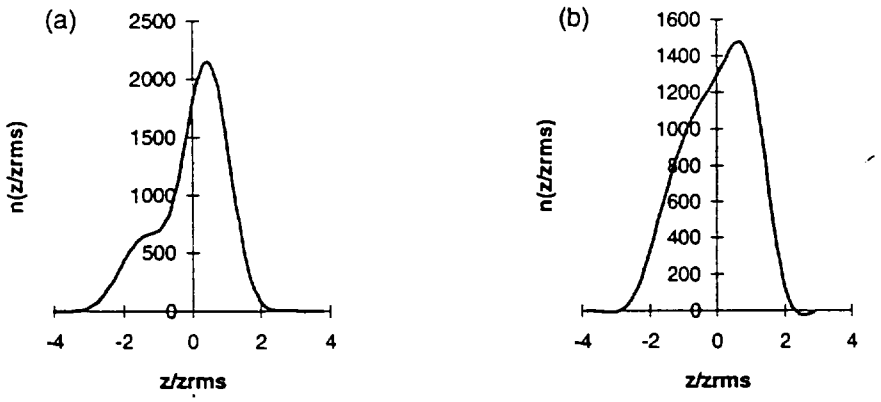


Figure 1 : The longitudinal beam density distribution n(z) for the CERN high current proton DTL [2]at 213 mA (a) and for the CERN $Pb^{27+}$ ion interdigital H linac [3] at 10 mA (b).

Since it is difficult to check the range of validity and the accuracy of a space charge procedure, only comparisons between different space charge methods will be made. When differences occur, it is essential to inspect the main limitations of the different categories of space charge routines.

## II. A MODIFIED METHOD FOR SPACE CHARGE CALCULATION

This modified method, in the form of a routine called SCHERM, derives from the approach used in the 3-d MAPRO2 routine [4] and generalised in the SC3DELP routine [5].

In MAPRO2, developed at CERN and Saclay, the macroparticle distribution is represented at each step by a continuous Gaussian charge density with ellipsoidal symmetry, from which the space charge electric-field components could be calculated by numerical integration. The restriction to a Gaussian profile is in principle not compatible with realistic distributions in intense beams and could therefore lead to inaccurate calculations. The MAPRO2 method has been improved in the SC3DELP routine, developed at LANL, to describe charge densities in 3-d ellipsoids. It is however assumed that in transverse and longitudinal direction, the bunches keep an ellipsoidal shape. In addition, the computation of the particle density gives a zero divide on the centre, and must be artificially extended around this centre.

SCHERM, on the contrary, can compute non-symmetrical longitudinal distributions and properly handles the problem of zero divide on the centre.

### *II.1. Ellipsoidal Density Distribution Calculation*

The density distribution in a bunch along the longitudinal axis can take a complex non-symmetrical shape. In order to represent such shapes, SCHERM decomposes the original longitudinal distribution into two or more symmetrical distributions which are considered to be of ellipsoidal form ( fig. 2 ).

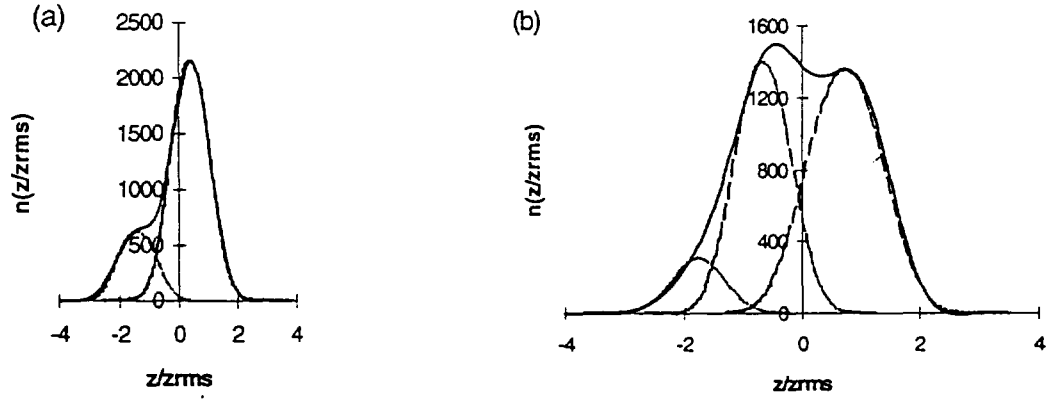


Figure 2 : Shown are the density distributions as in figures 1 a) and 1b) (continuous lines) with their computed decompositions in 2 or 3 ellipsoids (dashed lines).

Scaling the coordinates along the principal axes relative to the r.m.s. dimensions a, b, c for each of these ellipsoids, the distribution function n(x/a, y/b, z/c) becomes of a spherical type. For such a sphere ( see fig. 3 ), one can introduce its radial density distribution n(R) and also consider the density distribution for each individual coordinate by integration over the two others ( as in equation (1) ).

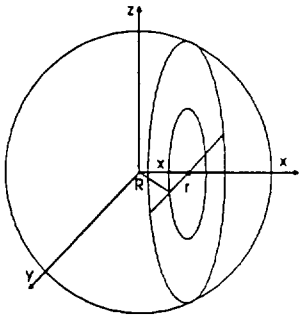


Figure 3 : Density distribution coordinates.

Referring to fig. 3 one has :

$$m_x\left(\frac{x}{a}\right) = m_y\left(\frac{y}{b}\right) = m_z\left(\frac{z}{c}\right) = \int n(R) 2\pi r dr \tag{1}$$

Let

$$R^2 = \left(\frac{x}{a}\right)^2 + \left(\frac{y}{b}\right)^2 + \left(\frac{z}{c}\right)^2 \equiv t \tag{2}$$

and

$$(x/a)^2 = u \tag{3}$$

$$r^2 = t\text{-}u \tag{4}$$

This gives, with constant x :

$$m_x\left(\frac{x}{a}\right) = \pi \int_u^{\infty} n(R) dt \tag{5}$$

With (4) and t to represent the radial variable R :

$$m_x(u) = \pi \int_u^{\infty} n(t) dt \tag{6}$$

From which one obtains

$$n(t) = -\frac{1}{\pi} \frac{dm_x(u)}{du} \tag{7}$$

where the density $m_x$ can be replaced by $m_y$ or $m_z$.

For the application of the above, instead of directly computing the particle density n(t) as in [5], one determines $m_x(x/a)$, $m_y(y/b)$ and $m_z(z/c)$, as explained in the next paragraphs. One takes the average value :

$$m(u) = \tfrac{1}{3}\left[m_x\left(\tfrac{x}{a}\right) + m_y\left(\tfrac{y}{b}\right) + m_z\left(\tfrac{z}{c}\right)\right] \qquad (8)$$

and subsequently applies a relation like (7). Moreover one can check that the terms in (8) are similar. Around the coordinate axis the densities are high and there is no singularity of $m_x(x/a)$ around x = 0 (similarly for y and z). By symmetry it is also true that : $m_x(-x/a) = m_x(x/a)$, and again similarly for y and z.

### *II.2. Hermite expansion of the density distribution*

The distributions in x, y and z for real beams (without well defined limits) resemble Gaussians, not only for low intensity beams but also at moderate and higher intensities. It is then appropriate to express these distributions in the form of a Hermite-series expansion, giving a good representation of the Gaussian appearance. Moreover it allows to reduce the statistical noise and avoids the oscillations from Fourier-series expansions of the SC3DELP routine.

Expressing each term in (8) with Hermite polynomials, one can write :

$$m_z\left(\tfrac{z}{c}\right) = \sum_i A_i \exp\left(-\tfrac{z^2}{2c^2}\right) H_i\left(\tfrac{z}{c}\right) \qquad (9)$$

and similar expressions for $m_x(x/a)$ and $m_y(y/b)$.

The coefficients $A_i$ are obtained with the orthogonality relationships. From :

$$\int_{-\infty}^{+\infty} \exp\left(-\tfrac{v^2}{2}\right) H_i(v) H_j(v)\, dv = \begin{cases} 0 & i \neq j \\ i!\sqrt{2\pi} & i = j \end{cases} \qquad (10)$$

one obtains :

$$A_i = \tfrac{1}{i!\sqrt{2\pi}} \int_{-\infty}^{+\infty} m_z\left(\tfrac{z}{c}\right) H_i\left(\tfrac{z}{c}\right) d\left(\tfrac{z}{c}\right) \qquad (11)$$

The integral above can be approximated as a summation over all N particles ; the number of particles in the length $\mathrm{d}\left(\frac{z}{c}\right)$ is :

$$\mathrm{dN} = m_z\left(\tfrac{z}{c}\right) \mathrm{d}\left(\tfrac{z}{c}\right) \qquad (12)$$

eq. (11) can be rewritten :

$$A_i = \tfrac{1}{i!\sqrt{2\pi}} \int_{\text{total length } z} H_i\left(\tfrac{z}{c}\right) dN \cong \tfrac{1}{i!\sqrt{2\pi}} \sum_{j=1}^{N} H_i\left(\tfrac{z_j}{c}\right) \qquad (13)$$

The Hermite polynomials $H_i(v)$ are obtained from the recurrence relation :

$$H_{i+1}(v) = v\,H_i(v) - i\,H_{i-1}(v) \tag{14}$$

The first few Hermite polynomials are given by :

$$\begin{aligned} H_0(v) &= 1 \\ H_1(v) &= v \\ H_2(v) &= v^2-1 \\ H_3(v) &= v^3-3v \\ H_4(v) &= v^4-6v^2+3 \\ &\cdots\cdots\cdots \end{aligned} \tag{15}$$

The Hermite polynomials $H_{2i}(v)$ are always even. It is then obvious that symmetrical distributions are only expressed with even Hermite-series polynomials. Proof of the above results and additional properties can be found in the literature.

It is significant to note that, assuming $m_z(z/c)$ is symmetrical around z = 0, one has :

$$A_2 = \frac{1}{\sqrt{2\pi}} \int_{z\geq 0} H_2\left(\frac{z}{c}\right) dN = \frac{1}{\sqrt{2\pi}} \left[ \int_{z\geq 0} \frac{z^2}{c^2} dN - \int_{z\geq 0} dN \right] \tag{16}$$

As the r.m.s. dimension c for a symmetrical distribution is given by :

$$c^2 = \frac{2}{N} \int_{z\geq 0} z^2 dN \tag{17}$$

we can write from eq. (16) :

$$A_2 = \frac{1}{\sqrt{2\pi}} \left[ \frac{N}{2} - \int_{z\geq 0} dN \right] = 0 \tag{18}$$

Then using the summation over all the N particles in eq. (13) with :

$$c^2 = \frac{2}{N} \sum_j z_j^2 , \quad z_j \geq 0 \tag{19}$$

one **must** obtain $A_2 \equiv 0$.

### *II.3. The longitudinal charge density and its decomposition into two (or more) ellipsoids*

It is usually assumed that the longitudinal density distribution is only decomposed into two or three ellipsoids. The procedure could however be easily extended to more.

The z-coordinates are relocated around the centre of gravity of the bunch. This distribution (not necessary symmetrical) is expressed with even and odd Hermite-series polynomials :

$$m_z\left(\frac{z}{c}\right) = \sum_n A_n \exp\left(-\frac{z^2}{2c^2}\right) H_n\left(\frac{z}{c}\right) \tag{20}$$

with

$$A_n = \frac{1}{n!\sqrt{2\pi}} \sum_{j=1}^{N} H_n\left(\frac{z_j}{c}\right) \tag{21}$$

c represents the z-r.m.s. dimension of the bunch :

$$c^2 = \frac{1}{N} \sum_{j=1}^{N} z_j^2 \tag{22}$$

The equation (21) is an approximation of eq. (11). Some isolated particles far from the centre of gravity (with great z/c values) can distort its accuracy. This is avoided by limiting the summation in eq. (21) to within 4 standard-deviations, i.e. such that $z/c \leq 4$.

Symmetrizing the denser part around the crest position $\hat{z}_1 / c$ as shown in fig. 4, one obtains a new symmetrical distribution $m_1(v)$, with $v=(z-\hat{z}_1)/c$

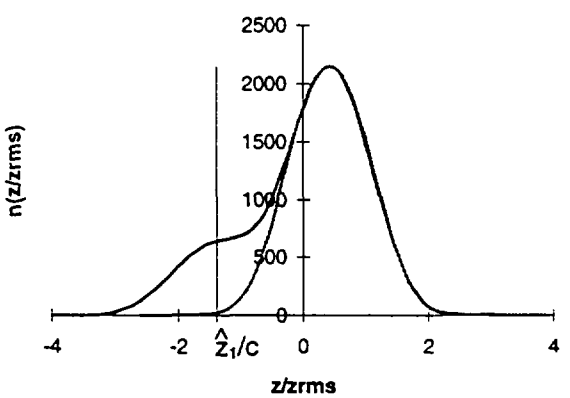


Figure 4 : The original longitudinal beam density distribution and the one of the main ellipsoid corresponding to $m_1(v)$.

There is a simple way to get the z-r.m.s. dimension $c_1$ of this new distribution ; in the case of fig. 4 one considers particles in the denser part such that :

$$z_j \geq \hat{z}_1$$

Let $N_1$ the number of these particles. One has :

$$c_1^2 = \frac{2}{N_1}\sum_{j=1}^{N_1}(z_j - \hat{z}_1)^2 \qquad (23)$$

However this can lead to inaccuracy when $N_1$ is small. It is then preferable to acquire this dimension from the original longitudinal distribution in eq. (20). This distribution has been obtained from the total number N of particles ($N \geq 2N_1$).

Using the Hermite expansion (20), one has :

$$c_1^2 = \frac{\int_{\hat{z}_1/c}^{\infty}(z-\hat{z}_1)^2 m_z(z/c)dz}{\int_{\hat{z}_1/c}^{\infty} m_z(z/c)dz} \qquad (24)$$

In order to express the symmetrical distribution $m_1(v)$ one can use even Hermite-series polynomials.

Let

$$v = \frac{z-\hat{z}_1}{c}, \quad z \geq \hat{z}_1 \qquad (25)$$

$$m_1(v) = \sum_n B_{2n}\exp\left(-\frac{v^2}{2}\right)H_{2n}(v) \qquad (26)$$

The Hermite coefficients are given by :

$$B_{2n} = \frac{2}{(2n)!\sqrt{2\pi}}\int_0^{\infty} m_1(v)H_{2n}(v)dv \qquad (27)$$

They could be approximated by :

$$B_{2n} = \frac{2}{(2n)!\sqrt{2\pi}}\sum_{j=1}^{N_1} H_{2n}(v_j) \qquad (28)$$

However these approximations could lead to inaccuracy when $N_1$ is small. It is better to compute these coefficients directly from the original longitudinal distribution given by eq. (20):

$$B_{2n} = \frac{2}{(2n)!\sqrt{2\pi}}\int_{\hat{z}_1/c}^{\infty} m(v)H_{2n}(v)dv \qquad (29)$$

These integrals are computed with Gaussian quadrature. The upper limits can be fixed to 4 (4 standard-deviations).

The same procedure can be applied to the remaining part of the original longitudinal distribution by the introduction of a second ellipsoid, representing the difference between m(v) and $m_1(v)$.

Referring to fig. 5, $\hat{z}_2 / c$ is the crest position of this difference.

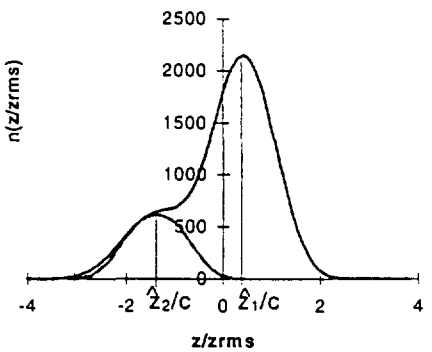


Figure 5 : The original longitudinal beam density distribution and the one of the second ellipsoid.

As above, symmetrizing the denser part of this difference around $\hat{z}_2 / c$, one gets the second symmetrical distribution $m_2((z - \hat{z}_2) / c)$. The z-r.m.s. dimension $c_2$ of this function is obtained in a similar way as $c_1$ in equation (24).

If the final residue can not be neglected ( i.e. if it represents more than 1 % of N) , a third ellipsoid is placed around the centre of gravity of this residue. Otherwise the final residue will be included in the second ellipsoid.

### *II.4. Computations of the Transverse Charge density distribution*

Contrary to the longitudinal motion, the transverse motion can be assumed symmetrical around the centre of gravity.

Let $m_x(x/a)$ and $m_y(y/b)$ be the original transverse densities in x and y respectively. With the coordinates x and y relocated about the centre of gravity, the r.m.s. dimensions are :

$$a^2 = \frac{1}{N}\sum_{j=1}^{N} x_j^2 \ , \ b^2 = \frac{1}{N}\sum_{j=1}^{N} y_j^2 \qquad (30)$$

respectively and the transverse distributions expanded with even Hermite-series polynomials are :

$$m_x\left(\frac{x}{a}\right) = \sum_n D_{2n} \exp\left(-\frac{x^2}{2a^2}\right) H_{2n}\left(\frac{x}{a}\right) \qquad (31)$$

$$m_y\left(\frac{y}{b}\right) = \sum_n E_{2n} \exp\left(-\frac{y^2}{2b^2}\right) H_{2n}\left(\frac{x}{b}\right) \tag{32}$$

with

$$D_{2n} = \frac{1}{(2n)!\sqrt{2\pi}} \sum_{j=1}^{N} H_{2n}\left(\frac{x_j}{a}\right) \tag{33}$$

and an identical expression for $E_{2n}$.

It can also be assumed that the behaviour of the transverse density distributions of the two or three ellipsoids is equivalent to the one of $m_x(x/a)$ and $m_y(y/b)$ of the bunch, from which they can be expressed.

One can define the fraction of particles in the first ellipsoid as :

$$S_1 = \frac{2 \int_{\hat{z}_1 / c}^{\infty} m_1(v)dv}{\int_{-\infty}^{+\infty} m_z(v)dv} \tag{34}$$

yielding to :

$$m_{1x}\left(\frac{x}{a}\right) = S_1 m_x\left(\frac{x}{a}\right) \tag{35}$$

$$m_{1y}\left(\frac{y}{b}\right) = S_1 m_y\left(\frac{y}{b}\right) \tag{36}$$

and identical relations for the second and third ellipsoid.

The functions $m_{1x}$ and $m_{1y}$ could also be obtained directly from the statistics. So the first ellipsoid concerns particles such that :

$$z_j \geq \hat{z}_1 \ , \quad j = 1,...N_1 \tag{37}$$

However, this causes irregularities due to statistical noise for the second and third ellipsoid when they are small.

*II.5. Hermite description of the macroparticle charge density*

Each particle is submitted to the field of two ellipsoids of charge distributions. For a uniformly charged ellipsoid, the particle density (number of particles per unit volume ) can be expressed as a function of a single generalised coordinate t :

$$n(t) = n\left(\frac{x^2}{a^2} + \frac{y^2}{b^2} + \frac{z^2}{c^2}\right) \tag{38}$$

The generalised coordinate of the first ellipsoid is :

$$t_1 = \frac{x^2}{a^2} + \frac{y^2}{b^2} + \frac{(z-\hat{z}_1)^2}{c_1^2} \tag{39}$$

and similarly ones for the second and third ellipsoid.

These quantities describe the isodensity contours of the distributions. They define families of concentric ellipsoids as $t_1$, $t_2$ vary from 0 to $\infty$. The advantage of the ellipsoidal distributions is that the electric field components can be expressed as a weighted integral over the particle-density distribution. Once the r.m.s. dimensions a, b, $c_1$ and $c_2$ have been calculated, the values of the generalised coordinates $t_1$, $t_2$ can be obtained for any coordinates x, y and z.

For the first ellipsoid the average value given in eq. (8) (see also fig. 6a) can be written as :

$$m_1(u) = \frac{1}{3}\left[m_{1x}\left(\frac{x}{a}\right) + m_{1y}\left(\frac{y}{b}\right) + m_{1z}\left(\frac{z-\hat{z}_1}{c_1}\right)\right] \tag{40}$$

Similar expressions can be found for the second and third ellipsoid. Eq. (7) and (8) allow the computation of the ellipsoidal density distribution :

$$n_1(t_1) = -\frac{1}{\pi}\frac{dm_1(u)}{du} = -\frac{1}{3\pi}\left[\frac{dm_{1x}(\sqrt{u})}{du} + \frac{dm_{1y}(\sqrt{u})}{du} + \frac{dm_{1z}(\sqrt{u})}{du}\right] \tag{41}$$

with a similar expression for $n_2(t_2)$ and $n_3(t_3)$.

From eq. (20) one has :

$$m_{1z}(\sqrt{u}) = \sum_n B_{2n} \exp(-\tfrac{u}{2}) H_{2n}(\sqrt{u}) \tag{42}$$

Identical expressions are obtained from eq. (31) and eq. (32).

With :

$$\frac{dH_{2i}(\sqrt{u})}{du} = \frac{1}{2}u^{-1/2}(2i)H_{2i-1}(\sqrt{u}) \tag{43}$$

the eq. (41) can be rewritten :

$$n_1(t_1) = -\frac{1}{6\pi}\sum_n 2n(S_1.D_{2n} + S_1.E_{2n} + B_{2n})H_{2n-1}(\sqrt{u})u^{-1/2}\exp\left(-\frac{u}{2}\right)$$
$$+\frac{1}{6\pi}\sum_n (S_1.D_{2n} + S_1.E_{2n} + B_{2n})H_{2n}(\sqrt{u})\exp\left(-\frac{u}{2}\right) \tag{44}$$

with similar expressions for $n_2(t_2)$ and $n_3(t_3)$. A graphical presentation is given in fig. 6b.

Posing :

$$H^*_{2n-1}(\sqrt{u}) = u^{-1/2}H_{2n-1}(\sqrt{u}) \ , \tag{45}$$

with eq. (14) one can find the following recurrence relation :

$$H^*_{2n-1}(\sqrt{u}) = H_{2n-2}(\sqrt{u}) - (2n-2)H^*_{2n-3}(\sqrt{u}) \tag{46}$$

The first few functions are given by :

$$H^*_1(\sqrt{u}) = 1$$
$$H^*_3(\sqrt{u}) = u - 3 \tag{47}$$
$$H^*_5(\sqrt{u}) = u^2 - 10u + 15$$

One can see that $n_1(t_1)$ is defined even when the isodensity contour $t_1$ falls to zero.

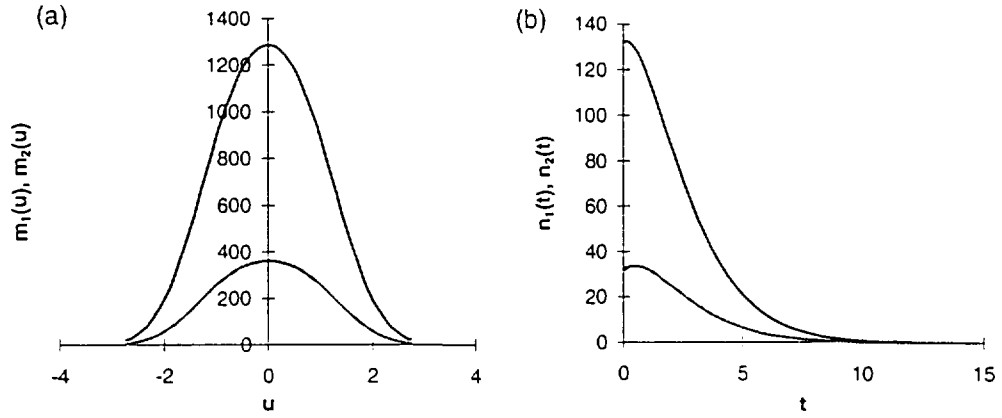


Figure 6 : The average values $m_1(u)$ and $m_2(u)$ are shown (a) with their corresponding macroparticle densities $n_1(u)$ and $n_2(u)$ (b) at a gap in the CERN proton linac.

### *II.6. Computation of the Electric Fields*

The three components of the electric field caused by an ellipsoidal distribution of charge $q^*$ can be expressed in terms of the density by the relation :

$$E_x = \frac{q^* abc\, x}{2\varepsilon_0} \int_0^\infty \frac{n(t)ds}{(a^2+s)^{3/2}(b^2+s)^{1/2}(c^2+s)^{1/2}} \; ; \qquad (48)$$

analogous expressions are valid for $E_y$ and $E_z$. Here the macroparticle charge $q^*$ will be calculated from :

$$q^* = \frac{I}{Nf} \qquad (49)$$

I is the average current in Amperes, f is the bunch frequency in Hertz, N is the total number of macroparticles and t is such that :

$$t = t(x,y,z,s) = \frac{x^2}{a^2+s} + \frac{y^2}{b^2+s} + \frac{z^2}{c^2+s} \qquad (50)$$

Assuming the original bunch distribution is decomposed into two or more ellipsoidal distributions, the three field components $E_x$, $E_y$ and $E_z$ produced by the bunch are the sum of each of these components for the ellipsoidal distributions.

These components can be determined by numerical integration as explained in [5] ; by changing to a new variable u such that :

$$s = d_1^2\left(\frac{1}{u} - 1\right) \qquad (51)$$

where

$$d_1 = (abc_1)^{1/3} \tag{52}$$

is chosen equal to the geometric mean of the r.m.s. size of the ellipsoidal distribution and is a scaling factor required to make the integral dimensionless.

The integration limits of the field integral are then transformed into 0 and 1, giving the new expression for the field :

$$E_z^{(1)} = \frac{q^*(abc_1)(z-\hat{z}_1)}{2\varepsilon_0} \int_0^1 n(t) u^{1/2} \frac{du}{d_1^3 \left[\left(\frac{a_1^2}{a_1^2}-1\right)u+1\right]^{1/2}\left[\left(\frac{b_1^2}{a_1^2}-1\right)u+1\right]^{1/2}\left[\left(\frac{c_1^2}{a_1^2}-1\right)u+1\right]^{1/2}} \tag{53}$$

Analogous expressions are obtained for the other field components for each of the ellipsoidal distributions.

The integral in eq. (53) is calculated using Gaussian numerical integration. Six field components must be computed for each macroparticle in the bunch. Beam simulations usually consider several thousands of macroparticles traversing throughout a linac. It is therefore essential to reduce the computer CPU time without lacking in accuracy.

The computer CPU time for each field integral depends on the number of Gaussian points required for the integration and on the number of terms involved in the Hermite-series expansions of the macroparticle charge density n(t) (see eq. (44)).

Only even terms appear in the macroparticle charge density description. Moreover it has been said that these terms are null for n = 2 ($B_2 = C_2 = D_2 = E_2 = 0$). Due to the factorial term in the denominator as shown for instance in eq. (27), the Hermite coefficients decrease rapidly to zero when n increases ( fig.7 ) and therefore only three coefficients ( i.e. n=4 ) are considered in the summation of eq. (44).

One observes in eq. (44) existence of functions as :

$$K_{2n}(v) = H_{2n}(v)\exp(-v^2/2) \tag{54}$$

and

$$K^*_{2n-1}(v) = v^{-1}H_{2n-1}(v)\exp(-v^2/2) \tag{55}$$

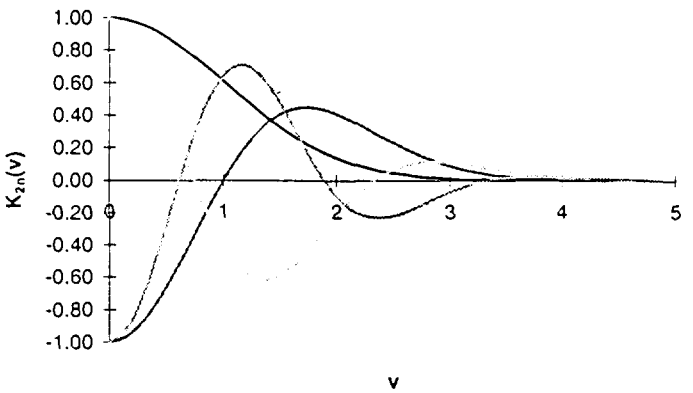


Figure 7 : $K_{2n}(v)$ is shown for n = 0 to 3. They decrease rapidly to zero and might be considered null when $v \geq 4$ (corresponding to 4 standard-deviations).

The small variation of n(t) in eq. (53) induces a regular variation of the function in the integral and no more than 5 or 6 Gaussian points are needed.

## III. OTHER SPACE CHARGE ROUTINES

Space charge routines have been classified into three categories, SCHERM belonging to the third one. The effect of adjacent bunches is computed as in the other routines. In order to treat non-symmetrical distributions, the macroparticle is represented by two (or more) ellipsoidal distributions. As a consequence the computer CPU time required by SCHERM with two or three ellipsoids is roughly two to three times the one of SCHERM with one ellipsoid ( SCHERM with two ellipsoids needs roughly the same CPU time as SC3DELP; which also uses one ellipsoid; this will be discussed later). It will be important to check that the extra CPU time required by SCHERM is worthwhile in view of the accuracy of the calculations.

As it has been said, the difficulty is to detect directly the most representative and correct approach. Comparisons with other space charge routines must be made, particularly with the ones applying other techniques such as PIC or PPI methods.

Several 3-d PPI routines have been developed : MAPRO1 [4], MOTION [6] and by Los Alamos [7], all based on interactions between finite-sized spherical clouds rather than point-to-point interactions. A disadvantage of these methods is that they are strongly subject to statistical noise. They need a great number of macroparticles and they are very time consuming on the computer.

A very elaborate PIC routine SCHEFF has been developed at LANL, partially avoiding these drawbacks. This routine, introduced in the code PARMILA [8], benefits from many improvements as the result of many calculations in high intensity beam dynamics. The routine SCHEFF is an excellent candidate for comparative computations with our new space charge

procedure. In order to explain the differences which could arise in these comparisons, it is essential to examine the limits of SCHEFF. This inspection requires an exact knowledge of the fundamental principle of this routine. Since it is difficult to find a reference in literature giving precise information about the SCHEFF method, it is briefly described here.

### *III.1. Description of SCHEFF principle*

This method is based on the following powerful property : any distribution presenting a rotational symmetry around an axis can be developed in rings of elementary charge. Each ring can be assigned a potential; superposing these potentials one obtains a suitable value of the potential at any point.

A 2-d r-z mesh ( one uses the cylindrical coordinates r, $\varphi$, z ) of a given size is placed on the bunch. For particles outside this mesh one estimates the space charge impulse based on a point of charge at the centre of the bunch. For the particles inside the mesh one proceeds as follows : Referring to fig. 8, $T = \pi(r_{k+1}^2 - r_k^2)dz$ is the volume of the ring corresponding to the rectangular surface $S = (r_{k+1} - r_k)dz$. This surface is assumed to be uniformly charged.

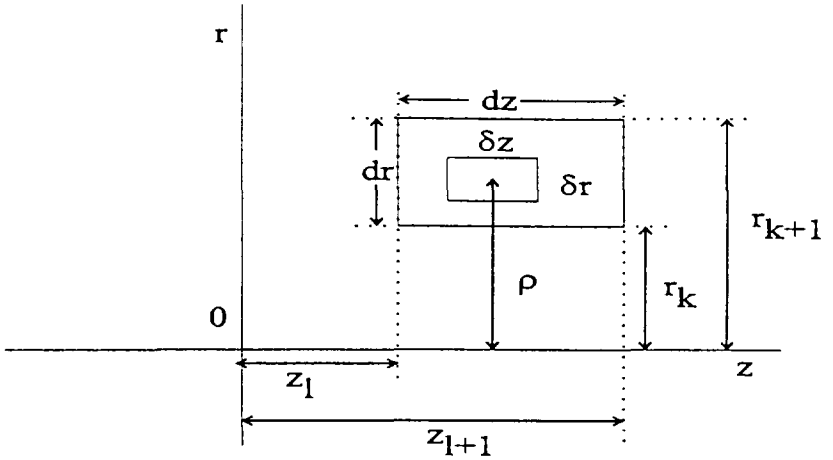


Figure 8 : Cut of the elementary ring of charge distribution in the mesh.

The elementary ring generated from the surface $\delta S = \delta r\, \delta z$ inside S can be assumed equivalent to a circle of radius $\rho$ ($r_k \le \rho \le r_{k+1}$) and of a uniform density of charge $\lambda$ such that:

$$\lambda = \frac{2\rho\delta z\delta r}{(r_{k+1}^2 - r_k^2)dz} \tag{56}$$

(the charge is assumed to be unity). This circle produces at the point P(R,z) (see fig. 9) the potential :

$$\delta V = \frac{\lambda\rho}{2\pi\varepsilon_0}\int_0^{\pi}\frac{d\varphi}{r} \tag{57}$$

r, as indicated in fig. 9, is the distance $\overline{MP}$.

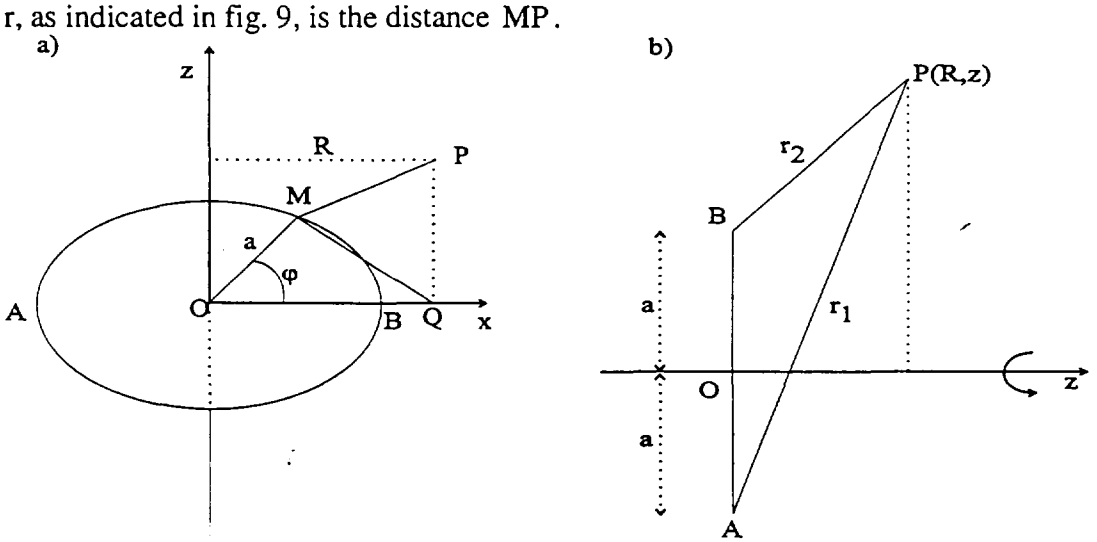


Figure 9 : The coordinates used for the computation of the potential produced in P by the ring M are shown in a). $r_1$ and $r_2$ are defined in b).

One has :

$$\overline{MP} = r = \sqrt{z^2 + \overline{MQ}^2} = \sqrt{z^2 + \rho^2 + R^2 - 2\rho R\cos\varphi} \tag{58}$$

R as shown in fig. 9 represents the distance from the point P to the rotational axis $o\vec{z}$ .

One now introduces a new variable θ such that :

$$\varphi = \pi - 2\theta \text{ , then } d\varphi = -2d\theta \tag{59}$$

With this new variable, eq. (58) can be rewritten :

$$r = \sqrt{z^2 + (\rho + R)^2 - 4\rho R \sin^2\theta} \tag{60}$$

Let

$$k = \sqrt{\frac{4\rho R}{z^2 + (\rho + R)^2}} = \frac{2\sqrt{\rho R}}{r_1}, \tag{61}$$

where :

$$r_1 = \sqrt{z^2 + (\rho + R)^2}$$

With this variable, eq. (57) takes on the form :

$$\delta V(z, R) = \frac{\lambda\rho}{\pi\varepsilon_0}\frac{1}{r_1}J_1(k) \tag{62}$$

where :

$$J_1(k) = \int_0^{\pi/2} \frac{d\theta}{\sqrt{1 - k^2\sin^2\theta}} \tag{63}$$

is the Legendre integral of the first kind, and one has :

$$\delta V(z, R) = \frac{\lambda\rho}{\pi\varepsilon_0}\frac{J_1(k)}{r_1} \tag{64}$$

Deriving this potential with respect to R and z, one obtains the space charge electric fields induced by the elementary ring :

$$\delta E_r = -\frac{\partial \delta V}{\partial R}, \quad \delta E_z = -\frac{\partial \delta V}{\partial z} \tag{65}$$

After some elaborate calculations, one gets :

$$\delta E_r = \frac{\lambda\rho}{\pi\varepsilon_0}\frac{1}{2r_1 R}\left[J_1(k) - \frac{\rho^2 - R^2 + z^2}{r_1^2}\frac{J_2(k)}{1 - k^2}\right] \tag{66}$$

$$\delta E_z = \frac{\lambda\rho}{\pi\varepsilon_0}\frac{z}{r_1^3}\frac{J_2(k)}{1 - k^2} \tag{67}$$

with δ z as in fig.8 and with $J_2(k)$ the Legendre integral of the second kind :

$$J_2(k) = \int_0^{\pi/2} \sqrt{1 - k^2 \sin^2\theta}\, d\theta \qquad (68)$$

The ring of charge due to the surface S generates the space charge fields $E_r$, $E_z$ at node P as obtained from eq. (66) and eq. (67) by double integration in the r - z space :

$$E_r(r_p, z_p) = \int_{r_k}^{r_{k+1}} \int_{z_1}^{z_2} \delta E_r(r, z) \qquad (69)$$

where $r_p$ and $z_p$ are the coordinates of the node P where the field is computed. $r_k$ and $r_{k+1}$ correspond to the boundary of the box of charge considered ( see fig. 8 ). $z_1$ and $z_2$ are the distances of the node P with respect to the box boundaries. An identical relation is used for $E_z(r_p, z_p)$. In SCHEFF the integrations (69) are made numerically.

The $E_r$ and $E_z$ fields of each ring on each node are computed for a given z. This is repeated for $n_z$ positions and the obtained fields are then arranged in two tables, each of which requires $n_r * n_r * 2 * n_z$ memory reservations; $n_r$ being the number of node coordinates in the r direction and $2 * n_z$ in the z direction.

The next step is to calculate the field contribution of each macroparticle to each node in order to take into account the macroparticle distribution in the bunch. The coordinates of the macroparticle j are $\bar{r}_j, z_j$, where $\bar{r}_j$ is an average radius such that :

$$\bar{r}_j = \sqrt{x_j^2 \frac{b}{a} + y_j^2 \frac{a}{b}} \qquad (70)$$

with a, b the transverse r.m.s. dimensions of the bunch.

To calculate the contribution of this macroparticle to the nodes of the mesh, its macrocharge (given by eq. (49)) is distributed on the nodes of the box in which it is located (according to its distance to these nodes) as well as on the nodes of the adjacent boxes. The field contribution of this macroparticle can then be computed from the precalculated field values. The total field at each node is then the sum of the field contributions of all macroparticles of the bunch.

From the fields at the nodes the impulse acting on a particle is then evaluated, using a smooth interpolation from node to node. Since such fields are computed for a case of rotational symmetry, a correction must be applied; in real space, the two components $E_x$, $E_y$ are given by the empirical relations :

$$E_x = E_{\bar{r}} \frac{2}{\sqrt{\frac{a}{b}} + 1} \qquad (71)$$

$$E_y = E_{\bar{r}} \frac{2}{\sqrt{\frac{b}{a}} + 1} \qquad (72)$$

Here $\bar{r}$ is the average radius in eq. (70). As the relations above eliminate coupling effects between x and y, they tend to reduce the transverse emittance growth.

### *III.2. Limitations inherent to the various space charge routines*

Comparisons have been made between SCHERM, SCHEFF, SC3DELP, and SCHERM with one ellipsoid (as SC3DELP but with Hermite-series expansions instead of Fourier-series expansions for the computation of the particle density). In order to perform the comparisons in an identical context, these routines have been introduced in the code DYNAC.

The space charge routines share the same main drawback ; the impulses from space charge are computed from a limited number of particles (a few thousand or few ten thousand) negligible in regard of the huge number present in the bunches. This deficiency in the sampled population is compensated by replacing the point like particles by a set of sources of more regular distributions, from which the space charge forces are calculated. These computations however are only feasible for a couple of geometrical distributions : spheres as in the PPI method, rings of charges as in SCHEFF, or ellipsoids as in SC3DELP and SCHERM.

#### *III.2.1. Limitations observed in the SCHEFF routine*

It has been explained that the SCHEFF method introduces a set of rings from which the space charge fields are calculated at discrete r-z mesh points. The impulse applied to a particle is given by a smoothing interpolation from the nodes of the box where it is located.

A large fraction of the fields $E_{r,k}$ and $E_{z,k}$ on the node k arises from the ring of charged macroparticles found in the boxes adjacent to this node. An insufficient number of macroparticles or an artificial inhomogeneity of the sampled population can have as a consequence that these boxes contain no particles, leading to very small fields at the node k. Holes will then appear in the applied impulse, as in fig. 10. Also the emittance growth and transmission are affected by the lack of statistics (fig. 11 ).

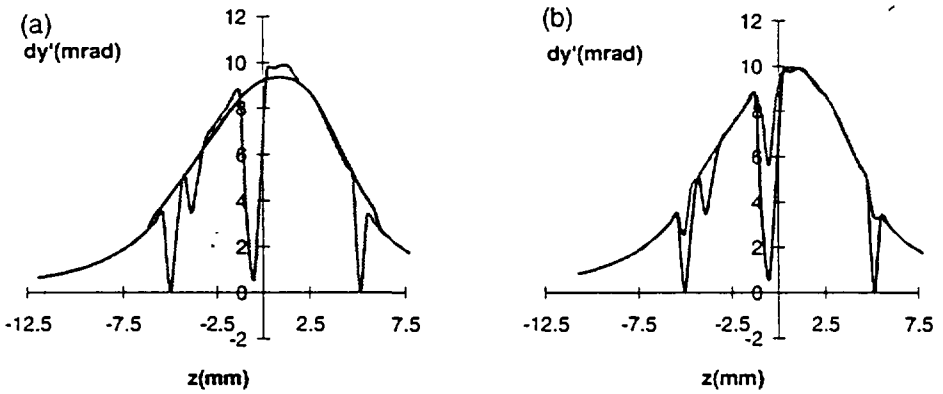


Figure 10 : SCHEFF results : In (a) the impulse dy', resulting from the field $E_y$ as a function of the z-coordinate of the bunch at the position x = 0 and y = 2b (b is the y-r.m.s. dimension of the bunch) for two different statistics : one for 1000 particles (light curve) and one for 5000 particles (dark curve). Note that with the bigger statistic the irregularities of the smaller one disappear. In (b) the impulse dy' as above for a statistic of 1000 particles (dark curve), and also for this same statistic increased sizes for dr and dz of the rectangle (see fig.8), with the total

mesh size kept constant (i.e. an decreased number of cells ; light curve). The irregularities are reduced, but persist.

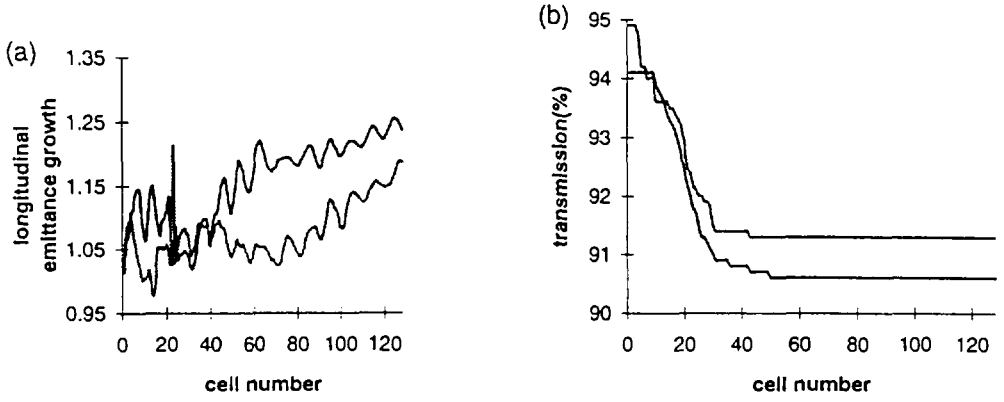


Figure 11 : SCHEFF results: In (a) the emittance growth ( i.e. current emittance divided by input emittance ) in the x-x' plane and in (b) the transmission for the CERN proton DTL (after having passed the matching section) as computed with SCHEFF for two different statistics : 1000 particles (light curves) and 5000 particles (dark curves).

In order to increase the accuracy when the number of particles is large, one might increase the number of nodes and fit at each step the r-z dimensions of the mesh to the ones of the bunch. However, additional nodes require a large amount of extra computer memory. SCHERM employs orders of magnitude less memory, with a greater consistency in the computational results.

In the DYNAC version of SCHEFF, the size of the mesh in r and z is adapted to the r.m.s. dimensions of the bunch at each step, keeping the number of nodes constant. However, reducing the mesh size by about 12 %, produces as seen in fig. 12, a significant change in the longitudinal emittance growth. The transverse emittance growth is hardly affected, nor is the beam transmission.

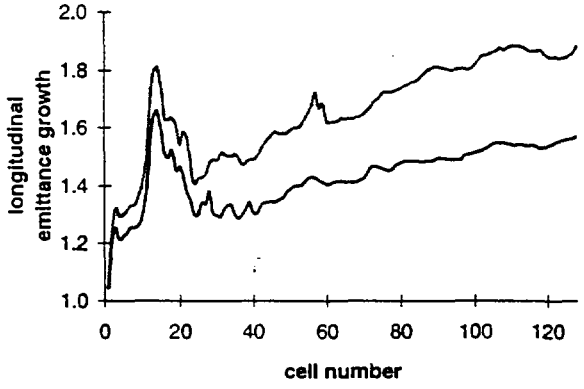


Figure 12 : Beam simulations with 5000 particles using SCHEFF with 2 different mesh sizes. Note the significant difference in emittance growth.

An other disadvantage of the SCHEFF method is that it uses rotational symmetry of the particle distribution around the axis for the computations. It is then restricted to those locations where the transverse beam cross section is close to round. However, the error resulting from the absence of circular symmetry is partially corrected by using the average

radius given in eq. (70) and the field expressions given in eq. (71) and eq. (72). The computations performed in the middle of quadrupoles, comparing the SCHEFF routine to the methods of the third category, which can treat separately the transverse motion in x and y, have shown that SCHEFF calculations could be considered realistic when the ratio between a and b is less than ~ 1.5. This is generally the case in the quadrupoles of a DTL, with the exception of some places due to a slight mismatch. In the transport lines the ratio between a and b is often greater then 2 or 3 and sometimes can attain 5 or more, as is the case in the beam matching section separating the CERN proton RFQ and linac. Fig. 13 shows in a place where the ratio a/b is large, the transverse space charge repulsion in x and y as computed with SCHEFF and SCHERM. It is too large in one direction and too small in the other. The correction (72) applies exactly near the axis of the beam but should drop to 1 at larger distance: in SCHEFF correction (72) is applied only inside the mesh but not outside while in practice there is a progressive change.

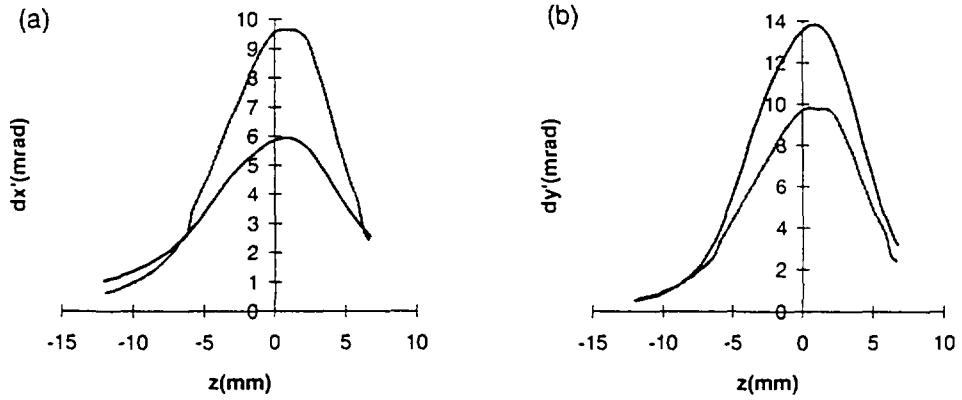


Figure 13 : In (a) the applied impulse dx' as a function of z for the position x = 2a and y = 0 ; in (b) the applied impulse dy' as a function of z for the position x =0 and y=2b. Both impulses are at the middle of a quadrupole in the matching line between the proton RFQ and linac at CERN, where b/a = 3.77.

*III.2.2. Limitations observed in SC3DELP and SCHERM with one ellipsoid*

In these two routines (of the last category) it is assumed that in transverse and longitudinal directions, the bunches keep an elliptical distribution. In SC3DELP as explained in [5], the macroparticle charge density is obtained from a direct approach (giving difficulty near the centre) and it is expressed with Fourier-series expansions. In SCHERM with one ellipsoid it is calculated with the approach given in paragraph II.1 (avoiding the difficulty near the centre), and Hermite-series expansions are employed. The advantage is the more regular variation of the macroparticle charge density representation (Fourier-series expansions can give oscillations), allowing the Gaussian numerical integration of eq. (53) with only 5 or 6 points, instead of 10 points for the same accuracy with Fourier-series expansions. The SC3DELP computing time is therefore almost twice as long as SCHERM with one ellipsoid and about the same as for SCHERM with two ellipsoids when only two ellipsoids are considered.

Nevertheless, a rather good agreement is obtained in the emittance growth and in the beam transmission with SC3DELP and SCHERM with one ellipsoid. The drawback of these routines results from the fact that in the longitudinal direction, the density distribution generally differs notably from a symmetrical form (in the CERN proton DTL, over a total of 128 cells, the bunches keep a symmetrical form in about 10 cells only), and superimposing a symmetrical shape could lead to incorrect calculation of the macroparticle charge density given in eq. (41). Applying this relation to the bunch, assumed be an ellipsoid ( $m_{lx}$ , $m_{ly}$ are the original transverse density distributions given in eq. (31) and eq. (32) ), $m_{lz}$ can then be obtained from :

$$m_{lz}\left(\frac{z}{c}\right) = \sum_n A_{2n} \exp\left(-\frac{z^2}{2c^2}\right) H_{2n}\left(\frac{z}{c}\right) \tag{73}$$

with

$$A_{2n} = \frac{1}{(2n)!\sqrt{2\pi}} \sum_{j=1}^{N} H_{2n}\left(\frac{z_j}{c}\right) \tag{74}$$

and c obtained from eq. (22).

Eq. (41) is only valid if the three terms in eq. (40) are similar. The symmetrical representation in eq. (73) of a non-symmetrical longitudinal density distribution could differ greatly from the ones of the transverse symmetrical distributions, and the eq. (41) could lead to wrong values of the electric fields components in eq. (53). In fig. 14 is shown the real distribution in the longitudinal direction, and the computed macroparticle charge density n(t) when the longitudinal density distribution is assumed symmetrical. The function n(t) falls off abnormally for $0 \leq t \leq 1$. It can even go down to zero.

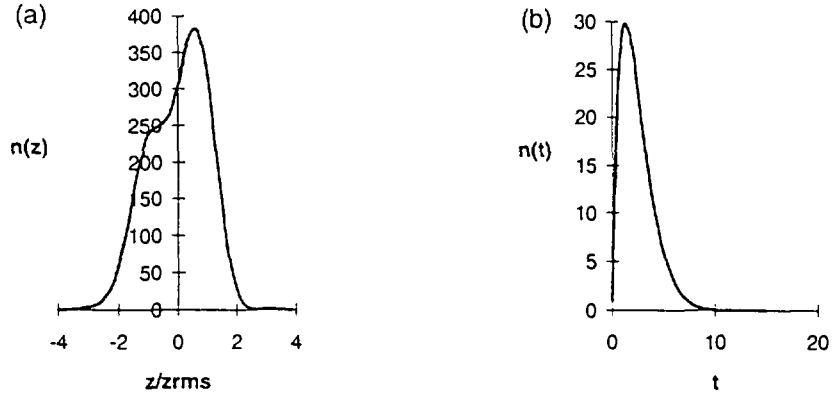


Figure 14 : In (a) a (asymmetrical) real macroparticle distribution in the longitudinal direction and in (b) the computed macroparticle charge density n(t) (in the computation the longitudinal density distribution was assumed symmetrical).

In fig. 15 on the contrary the longitudinal density distribution is rather symmetrical. The shape of the function n(t) is normal around t = 0, when the three terms in eq. (40) are similar.

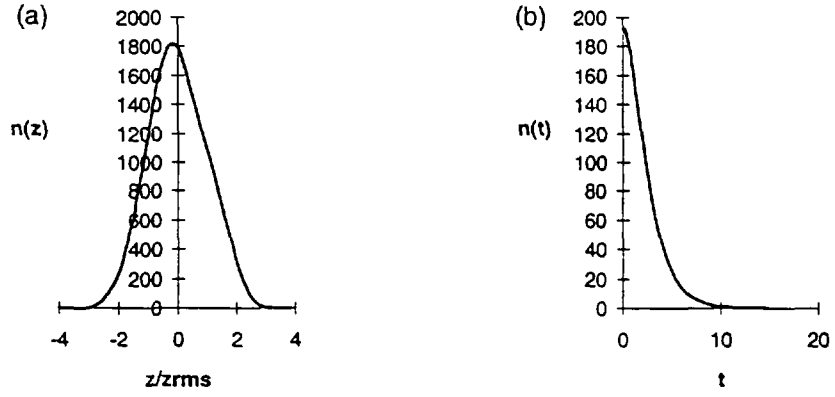


Figure 15 : In (a) the (symmetrical) real macroparticle distribution in the longitudinal direction and in (b) the computed macroparticle charge density n(t).

It is well known that a beam in a linac never keeps a well defined symmetrical form. The assumption that the bunches conserve an ellipsoidal distribution is not justified, and as explained above this can lead to inaccuracy, both in emittance growth as well as in beam transmission computations. In the next paragraph are shown comparative computations in a high beam intensity DTL, including these routines and the other methods developed in this article.

*III.2.3. Limitations observed in the SCHERM routine*

The stability of SCHERM results, in particular when the statistic changes or when the degree of Hermite-series polynomial is modified, must be checked. Using two very different statistics, one sees in fig. 16 quite good agreement in the emittance growth and in the beam transmission.

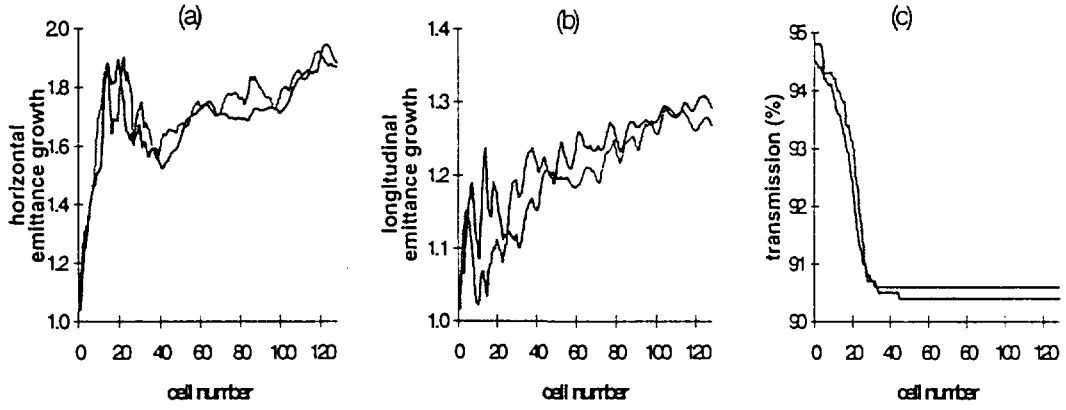


Figure 16 : The emittance growth in the horizontal (a) and longitudinal plane (b) as well as the transmission (c) as computed by SCHERM for the CERN proton linac for 2 different statistics : 1000 particles (light curve) and 5000 particles (dark curve).

In fig. 17 can be observed the small sensitivity of SCHERM computations to the degree of the even Hermite-series polynomials used.

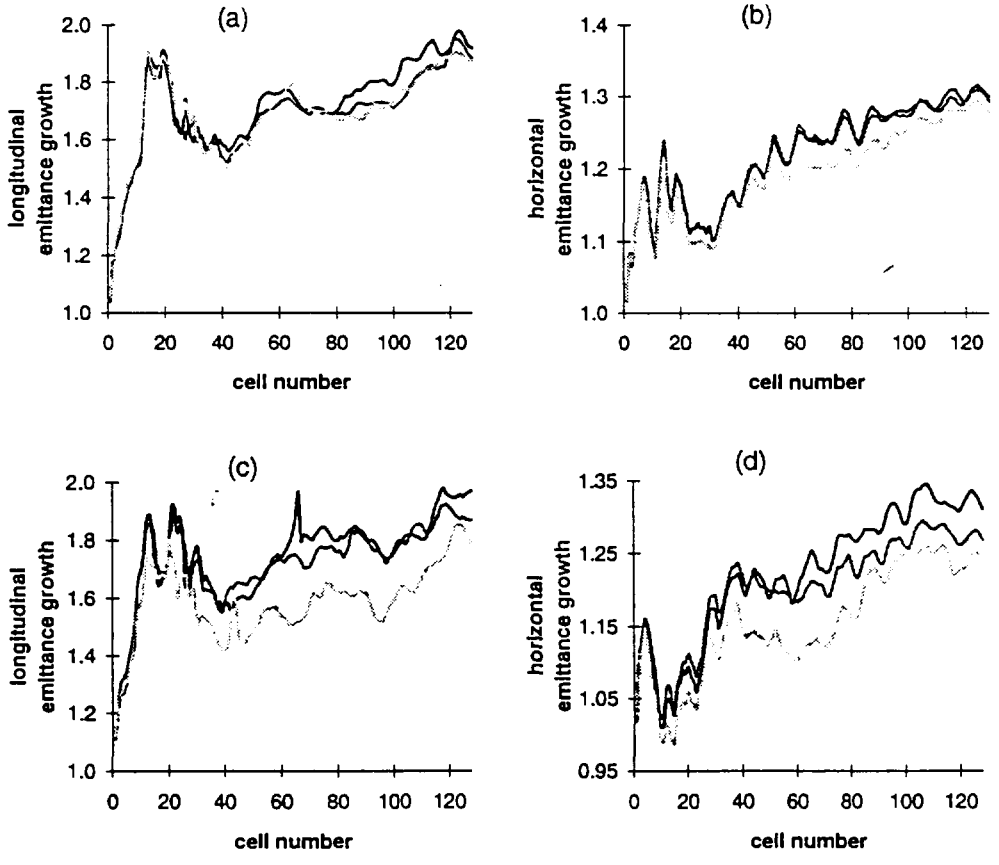

Figure 17 : In (a) and (b) the longitudinal and the horizontal emittance growth respectively, for a statistic of 5000 particles. The degrees of the Hermites polynomial in SCHERM computations are respectively 4 (light curve), 6 (darker curve) and 8 (darkest curve). (c) and (d) as (a) and (b), but with a statistic of 1000 particles.

Only 1000 particles and 3 terms in the Hermite-series polynomial ( i.e. of degree 0, 4, and 6 ) suffice.

In fig. 18 one can observe the relative similarity of the terms in eq. (8) necessary to justify the relation (7).

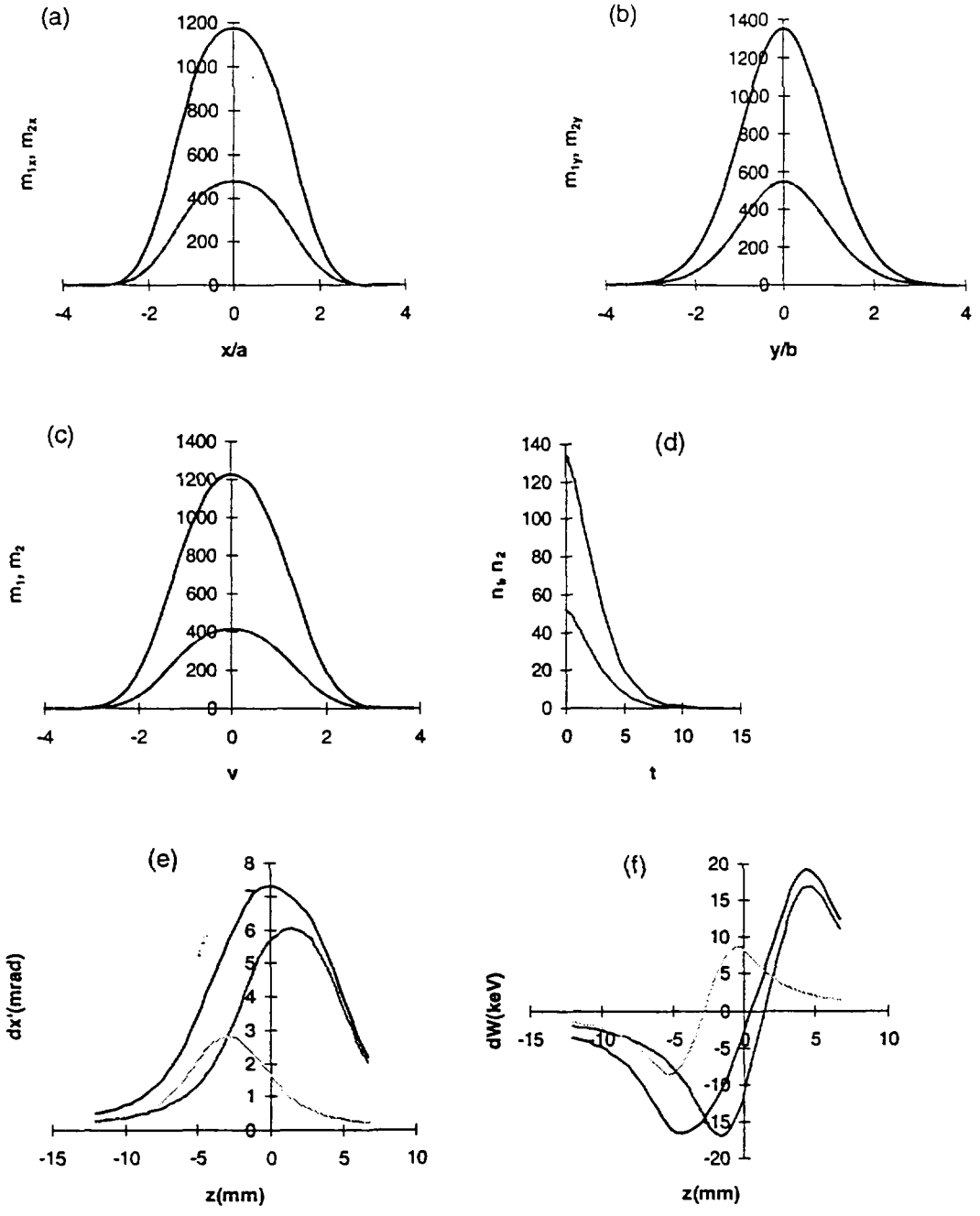


Figure 18 : The space charge computations are performed with the SCHERM routine in the middle of a quadrupole of the matching section between the CERN proton RFQ

and DTL. In (a) and (b) are the transverse charge distributions $m_{1x}$ , $m_{2x}$ (see eq.(35)), and $m_{1y}$ , $m_{2y}$ (see eq.(36)). In (c) are shown the longitudinal charge density $m_1(v)$ and $m_2(v)$ (see eq.(26)) and in (d) the macroparticle charge densities (eq.44). (e) and (f) show the impulses resulting from the fields Er and Ez of two ellipsoids (lighter curves) and their sum (dark curve).

## IV. CALCULATIONS WITH THE MODIFIED SPACE CHARGE ROUTINE AND COMPARISONS WITH OTHER PROCEDURES

Having seen the difficulties of the various space charge routines we shall now compare their results. We shall first compare the new routine SCHERM with the classical SCHEFF method and finally compare SCHERM type computations with one, two or three ellipsoids.

Concerning the comparisons, two different types of calculations will be made. One will consist in comparisons in emittance growth and beam transmission. Another will be to examine at different positions along the linac the impulses applied for various x and y values along the longitudinal direction of the bunch.

The CERN proton DTL has been chosen for our comparisons and the majority of the examples given are produced from this linac. This linac has been selected for its high beam intensity of 213 mA and the low proton input energy (of 750 keV). It has been operational for about 20 years and disposes of a lot of experimental measurement and a quantity of information on its behaviour. However, examples with another type of linac will also be provided.

### *IV.1. Comparisons between SCHERM and SCHEFF*

Applied in those locations where the beam cross section is round, the SCHEFF routine is a good candidate to compare SCHERM with. It does not require a hypothesis on the distribution in the longitudinal direction. However it has been explained that SCHEFF is sensitive to statistical effects and to the mesh size. It is obvious that this statistical noise affects the exact evolution of the beam.

A great number of comparative computations performed with different statistics allows to consider that using 5000 particles avoids the problems arising from the statistics (fig. 11). The same statistic has been taken for SCHERM, although 1000 particles would have been sufficient (see fig. 16).

In fig. 19 are shown comparisons of emittance growth and of beam transmission in the CERN proton DTL. There is a slight mismatch in the first tank (due to the high intensity of the beam), which the two space charge routines handle in a different way. This is due to the lack of rotational symmetry in a few places along the accelerator as well as to the incomplete linear correction applied in eq. (71) and (72). As a consequence one can observe a difference in emittance growth between the two methods.

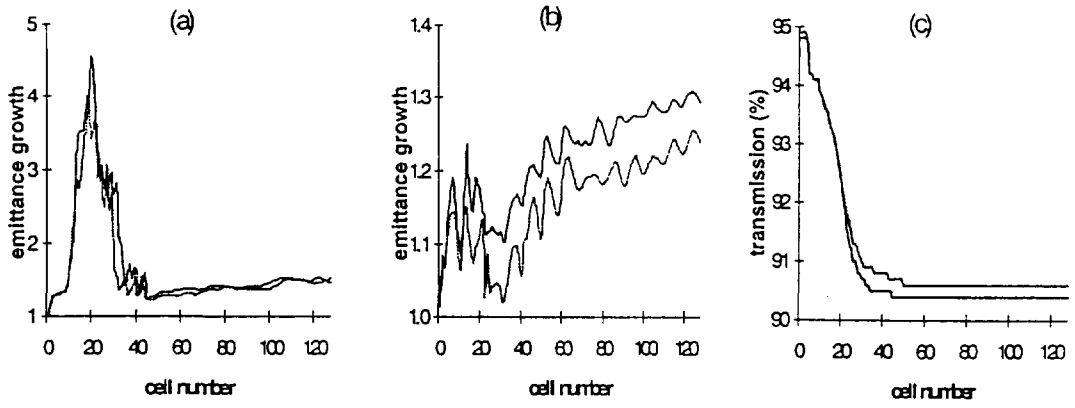


Figure 19 : Comparisons of emittance growth and beam transmission in the CERN proton DTL using SCHERM (dark curves) and SCHEFF (light curves). In (a) the longitudinal emittance growth and in (b) the horizontal emittance growth. In (c) the beam transmission is shown.

Another comparison of emittance growth and of beam transmission is given in fig. 20, for the interdigital H structure at CERN for acceleration of $Pb^{27+}$ . For the aim of comparison the beam intensity is 10 mA, quite out of the scope of the design of this machine.

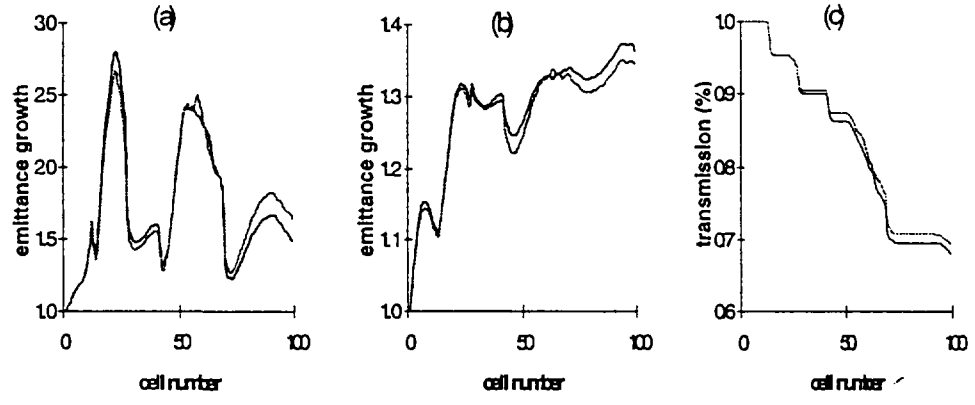


Figure 20 : Comparisons of emittance growth and of beam transmission for the interdigital H structure at CERN for acceleration of $Pb^{27+}$. (a),(b) and (c) are as in fig.19.

One can also compare at different positions along the accelerator (those located where the transverse cross section is roughly round) the impulses applied along the z and x or y direction of the bunch for various x and y values. Examples are given in fig. 21 for the CERN proton linac, and in fig. 22 for the CERN interdigital H structure.

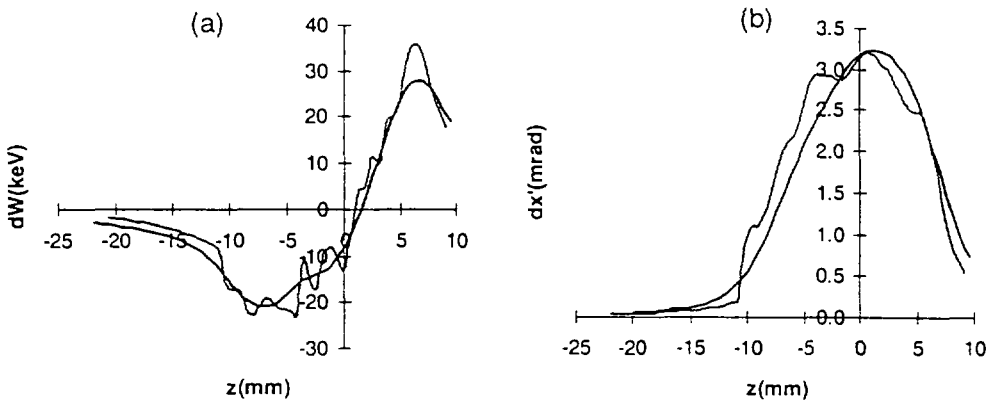


Figure 21 : In (a) comparisons for the CERN proton DTL of the impulses dW ( keV ) applied along the z direction for x=y=0. The dark curve represents SCHERM computations, the light curve the ones of the SCHEFF routine. In (b) as in (a), but for the impulses dx' ( mrad ) for x=0.8*a ( a is the x-r.m.s. dimension of the bunch ) and y=0. One remarks the erratic variations obtained with SCHEFF computations as a consequence of the interpolation from node to node.

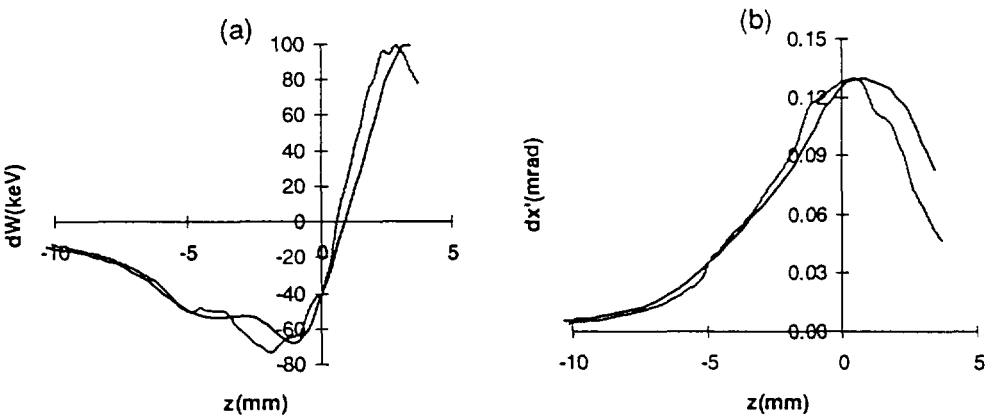


Figure 22 : Comparisons for the interdigital H stucture at CERN of the impulses applied along the z direction as in fig.21.

In fig. 23, 24 are represented the clouds of particles at the output of the CERN proton DTL, in the ( dPHI, dW) phase space and in the ( z, x ) plane for computations with SCHERM and SCHEFF. For the former routine one can see a cloud of particles in a kind of "winged butterfly" arrangement, which could be related to a halo phenomenon. It is not clearly seen for the latter routine as a consequence of the erratic variations in the SCHEFF computations seen in fig. 21, 22. However, as seen in fig. 19, the r.m.s emittance growth and the transmission are very similar.

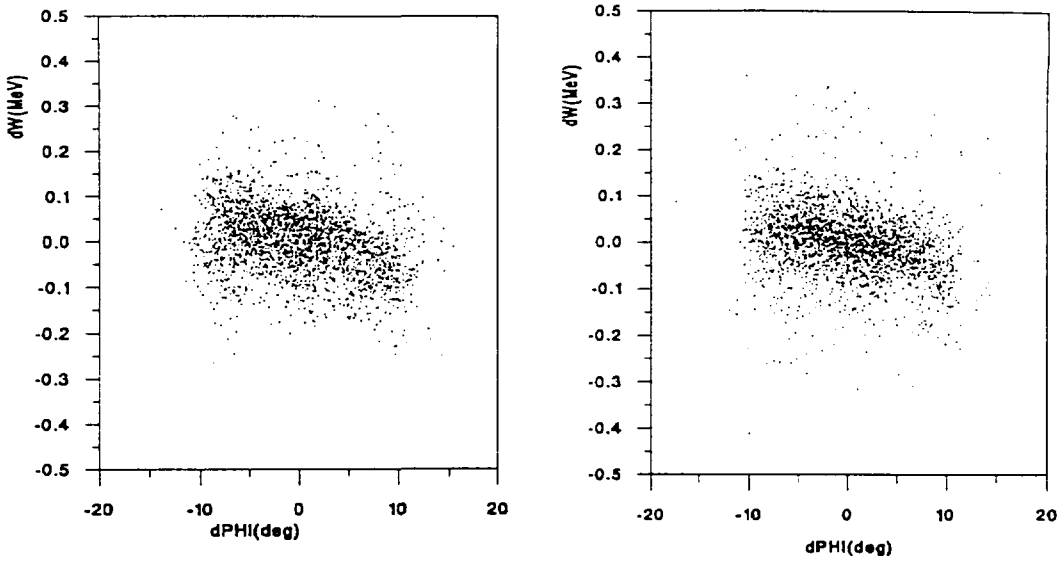


Figure 23 : In (a) the clouds of particles at the output of the CERN proton DTL in the phase space ( dPHI, dW ) for computations with SCHERM. In (b) as in (a) but for computations with the SCHEFF routine

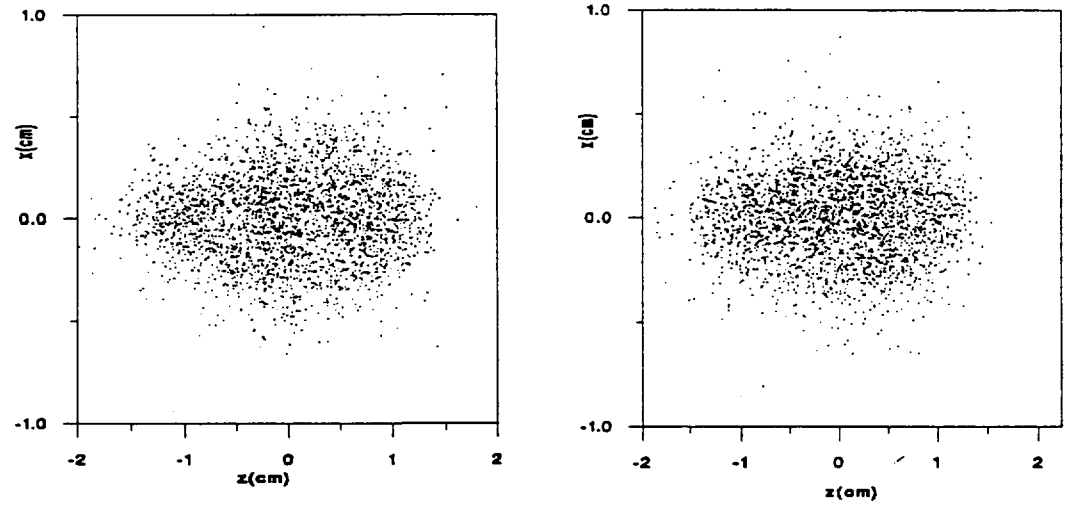


Figure 24 : In (a) are the clouds of particles at the output of the CERN proton DTL in the plane ( z, x ) for computations with SCHERM. In (b) as in (a) but for computations with the SCHEFF routine. One observes in (a) the presence of two clusters of particles, justifying the use of two ellipsoids. It is not clearly seen in (b).

### *IV.2. Comparisons between SCHERM with one and two ellipsoids and SC3DELP*

In fig. 25 are shown comparative computations between SCHERM with one and two ellipsoids, and SC3DELP for the emittance growth in the CERN proton DTL. Although significant differences are seen in the longitudinal emittance growth, the transmission rates are practically the same.

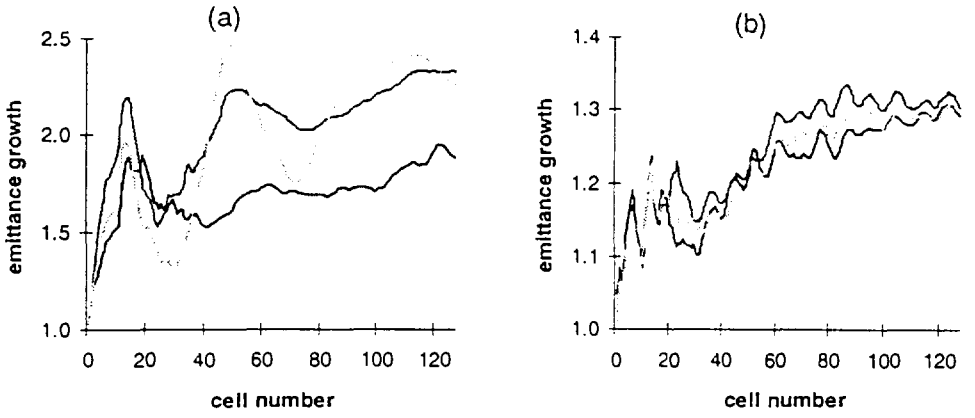


Figure 25 : Comparison of SCHERM with several ellipsoids (dark curves) to SCHERM with one ellipsoid (lighter curves) and SC3DELP (lightest curves). In (a) differences in longitudinal emittance growth occur due to the fact that the 1 ellipsoid procedure assumes a symmetrical beam. Good agreement, however, is found for the transverse emittance growth in (b).

## V. SPACE CHARGE COMPUTATIONS IN THE PRESENCE OF A BENDING MAGNET WITHOUT ISOCHRONICITY

Owing to the lack of isochronicity when the beam crosses a bending magnet, the bunch turns and its projection in the plane $(0\vec{z},0\vec{x})$ (or in the $(0\vec{z},0\vec{y})$ plane for a vertical bending ) rotates as shown in fig. 26.

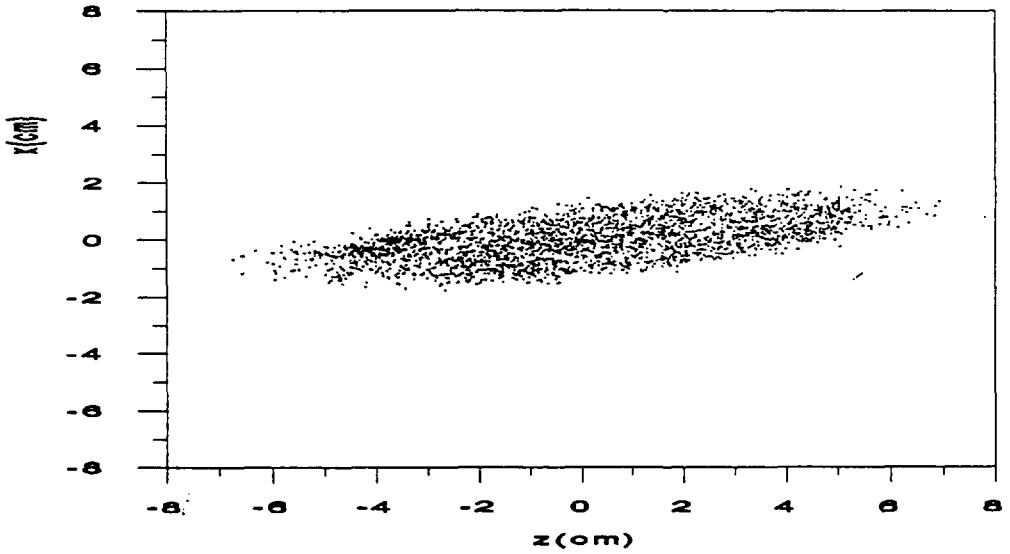


Figure 26 : A cloud of particles in the plane ( z, x ) for a beam crossing a bending magnet in the transport line after the CERN proton DTL.

Space charge computations as described so far are only feasible for an upright bunch, so it is necessary to define 2 new coordinate systems in which the bunch becomes erect.

The projection of the bunch in the plane $(0\vec{z},0\vec{x})$ is assumed to be of elliptical shape ( see fig 27 ).

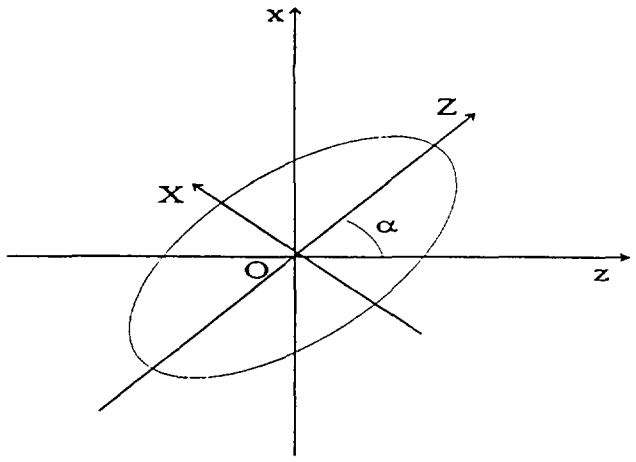


Figure 27 : The projection of the bunch in the plane ( z, x).

Let $0\vec{Z}$ and $0\vec{X}$ the principal axis of the ellipse. Its equation in the coordinate system $(0\vec{z},0\vec{x})$ is given by :

$$a_{11}z^2 + a_{12}\,xz + a_{22}x^2 + d = 0 \tag{75}$$

with :

$$\begin{cases} a_{11} = \frac{1}{N}\sum_i x_i^2 \\ a_{12} = \frac{1}{N}\sum_i x_i z_i \\ a_{22} = \frac{1}{N}\sum_i z_i^2 \end{cases} \tag{76}$$

The angle $\alpha$ between the positive x-axis and any principal axis of the ellipse satisfies the condition

$$tg2\alpha = \frac{2a_{12}}{a_{11}-a_{22}} \tag{77}$$

In the new coordinate system $(0\vec{X},0\vec{y},0\vec{Z})$ the bunch is erect and the components $E_Z$ and $E_X$ can be computed.

In the original coordinate system these components can be obtained with the following transformation :

$$\begin{pmatrix} E_z \\ E_x \end{pmatrix} = \begin{pmatrix} \cos\alpha & -\sin\alpha \\ \sin\alpha & \cos\alpha \end{pmatrix} \begin{pmatrix} E_Z \\ E_y \end{pmatrix} \tag{78}$$

Effects arising from misalignment leading to rotations in the planes $(0\vec{z},0\vec{x})$ and $(0\vec{z},0\vec{y})$ are generally weak and can often be neglected in space charge computations.

They cannot be omitted when the bunch passes through a dipole and the angle $\alpha$ can take significant values of about several tens of degrees, as can be seen in fig. 26.

## VI. COMPARISON OF COMPUTER CPU TIME FOR THE DIFFERENT SPACE CHARGE ROUTINES

A comparison of computer cpu time was made between the different space charge routines implicated. Concerning the SCHERM routines and the SC3DELP routine it has been said that the computer cpu time depends on the number of Gaussian points required for the integration of eq.(53). For the SCHERM routines it also depends on the number of terms involved in the Hermite-series expansions of the macroparticle charge density n(t) (see eq.(44)) and for the SC3DELP routine it also depends on the number of terms involved in the Fourier-series expansions of n(t). Three terms for n(t) and five Gaussian points are considered in the the summation of eq.(44) for the SCHERM procedures. It requires a five-term Fourier-series expansion to represent n(t), and 10 Gaussian points for the same accuracy in SC3DELP. In these routines, increasing the number of macroparticles N, the computer cpu time roughly increases as N.

In SCHEFF, a large amount of the computer cpu time is used to generate the fields Er and Ez (see eq.(69)). In the DYNAC version of SCHEFF these fields are computed at each step, as the sizes of the mesh are adapted to the r.m.s. dimensions of the bunch. The computer cpu time is then roughly proportional to the number of node coordinates in the r and z directions. In a lesser way it is also dependant on the number of particles.

It is obvious that the computer cpu time required depends on the type of computer. Therefore mainly the ratio of the computer cpu time of these different space charge routines is of interest.

Performing the computations with 5000 particles for the CERN proton DTL, one finds that the cpu time with the SCHERM method with two ellipsoids was roughly equal to the one of SC3DELP; it is about 1.6 times slower than SCHERM with one ellipsoid, and 2 times slower than SCHEFF ( computation for 20 nodes in the r direction and 40 in the z direction). Reducing the number of nodes in the SCHEFF routine by a factor 4 ( a factor 2 in each direction ), SCHERM with two ellipsoids is around three times slower than SCHEFF. This leads, however, to an increase in the size of dr and dz of the rectangles in the mesh ( see fig.8 ), with as consequence that the erratic variations of the applied space charge impulses become larger.

## VII. CONCLUSION

The SCHERM routine differs appreciably from the other space charge routines in several respects :

a) It can correctly compute space charge forces for a beam having both an asymmetric longitudinal particle distribution as well as a cross section without circular symmetry.

b) It is little sensitive to statistical noise and therefore gives significant results even when a small number of macroparticles is used ( 1000 or less ).

The more general approach mentioned under a) may turn out to be very useful to study halo formation; improvements to the method may, however, still be needed and are under development by the authors of this article. These improvements are beyond the scope of this article.

## VIII. ACKNOWLEDGEMENTS

We thank H. Haseroth and W. Pirkl from CERN and A. Tkatchenko from IN2P3-CNRS for their interest and support. We also want to thank D.Bunel from Saclay for her contribution.

## IX. REFERENCES

[1] P. Lapostolle, E. Tanke, S. Valero, "A New Method in Beam Dynamics Computations for Electrons and Ions in Complex Accelerating Elements", Particle Accelerators, 1994, Vol.44, pp.215-255

[2] D.J.Warner, "Accelerating Structure of the CERN New 50 MeV Linac", Proc. 1976 Linac Conf., AECL-5677, p49 (1976)

[3] Y.Bylinsky, H.Kugler, P. Lapostolle, U.Ratzinger, E. Tanke, S. Valero, D.Warner, "Dynamics and Tolerances for the CERN Inetrdigital H Linac", Proc. 1992 Linac Conf., AECL-10728, p220-222 (1992)

[4] M. Martini, M Promé, "Computer Studies of Beam Dynamics in a Proton Linear Accelerator with Space Charge", Part. Acc. 1971, Vol.2, pp. 289-299

[5] R.W. Garnett and T.P. Wangler, IEEE PAC Conf., San Francisco (1991),p.330-332

[6] K. Mittag, D. Sanitz, "MOTION, a Versatile Multiparticle Simulation Code", Linac Conf. Proc., Santa Fe, LA-9234-C, p.156 (1981)

[7] PPI de Los Alamos ??????????????????????????????????

[8] G.P. Boicourt, "PARMILA-An Overview", Linear Accelerator and Beam Optics Codes, AIP Conf. Proc, Vol. 177 (1988)

**Laboratoire National Saturne**

91191 Gif-sur-Yvette Cedex France
Tél : (1) 69 08 22 03
Téléfax : (1) 69 08 29 70
Bifnet : SATURNE @ FRCPN 11
Télex : ENERG X 604641 F